Crystal Structure of Ethylene−Vinyl Alcohol Copolymers

Masahide Takahashi,*,† Kohji Tashiro,*,‡ and Shigetoshi Amiya†

Analytical Research Center, Kuraray Co., Ltd., Kurashiki, Okayama 710-8691, Japan, and Department of Macromolecular Science, Graduate School of Science, Osaka University, Toyonaka, Osaka 560-0043, Japan

Received April 8, 1999; Revised Manuscript Received June 10, 1999

ABSTRACT: Crystal structures of ethylene−vinyl alcohol copolymers (EVOH) with various vinyl alcohol (VA) compositions have been determined on the basis of the X-ray diffraction data measured for the uniaxially and doubly oriented sample specimens. The unit cells of EVOH with a VA content higher than 27 mol % are monoclinic of the space group $P112_1/m$, in which the two planar-zigzag chains are statistically packed in a mode similar to that of poly(vinyl alcohol) (PVOH). With a decreasing VA content from 27 to 14 mol %, the crystal system approaches the hexagonol type. The unit cells of EVOH with a VA content below 14 mol % are orthorhombic of the space group *Pnam*, similar to the packing mode of orthorhombic polyethylene (PE). The crystal structure of EVOH with the VA content in the range of 14−27 mol % is the pseudohexagonal type. In this way the transformation of the unit cell structure between the PVOH type (>27 mol %) and PE type (<14 mol %) was found to occur via the appearance of a hexagonal-type structure. This transformation was supported also by the change in the infrared spectral pattern measured for a series of EVOH copolymers.

Introduction

The ethylene−vinyl alcohol copolymer (EVOH) has excellent gas-barrier properties and is used in various fields such as food packaging, gasoline tanks, or other materials.[1] EVOH is expected to work well as one of the soft materials for ecology because of no emission of poisonous gas upon incineration. This is because EVOH is composed of such elements as hydrogen, carbon, and oxygen and is chlorine-free. EVOH chains are constructed by random sequencing of hydrophobic ethylene (ET) and hydrophilic vinyl alcohol (VA) monomeric units. Therefore, the properties vary drastically with the copolymer composition. To understand the variation of physical properties with the VA content, it may be necessary to clarify the aggregation structure of chains in both the amorphous and crystalline regions and also in the so-called higher-order system. In particular, information on the crystal structure and its variation with VA content is needed first of all, which should give us the most basic and important guideline for the discussion of the bulk structure.

The crystal structure of poly(vinyl alcohol) (PVOH, VA = 100%)[2] and polyethylene (PE, VA = 0%)[3−5] were already determined by many researchers. The unit cell of PVOH is monoclinic with the space group $P112_1/m-C_{2h}^2$ where the chain axis is parallel to the *c* axis, while the unit cell of PE is orthorhombic with the space group $Pnam-D_{2h}^{16}$. PE also shows another type of crystal system, monoclinic[6] and hexagonal.[7−10]

All the members of EVOH copolymer samples with various VA compositions can be crystallized. The melting point varies continuously with the copolymer composition, suggesting that the crystal structure itself changes continuously with the change in the copolymer composition.

In the previously reported papers about the crystal structure of the EVOH copolymers,[11−13] the observed X-ray reflections were indexed and the continuous change in the lattice parameters with the VA content were described. Unfortunately, however, no trial had been made to analyze the X-ray diffraction intensities to obtain any information on the chain-packing mode for a series of EVOH crystals with the various VA contents. This information on the chain conformation and chain-packing mode in the crystal lattice may also be helpful for the quantitative interpretation of the crystallite modulus of a series of EVOH samples.[14] In this paper we will report the results of the crystal structure analysis made for a series of EVOH copolymers on the basis of the X-ray diffraction diagrams taken for the uniaxially oriented and the doubly oriented samples.

Experimental Section

Samples. Twelve kinds of EVOH copolymers with VA contents of 100, 95, 90, 68, 62, 56, 52, 41, 27, 14, 6, and 0 mol % were used in the present study. These samples are labeled as EVOH*mm* (e.g., EVOH68, etc.), where *mm* denotes the content of the VA unit in mol %. EVOH100 (PVOH) was the sample POVAL commercialized by Kuraray Co. Ltd., Japan. EVOH95∼EVOH41 were also the manufactured samples EVAL of the same company. EVOH27∼EVOH6 were prepared by saponifying the corresponding ethylene−vinyl acetate (EVAc) copolymers by methanolic KOH in benzene, where EVAc copolymers were commercial products of Monomer−Polymer & Dajac Labs, Inc., USA. The degrees of saponification were higher than 99% for all the copolymers. EVOH0 corresponds to high-density polyethylene (HDPE), a commercial product by Mitsui Chemicals Co. Ltd., Japan.

The uniaxially oriented samples were prepared for the X-ray structure analysis. EVOH100−EVOH90 films were cast from the 10 wt % aqueous solutions at room temperature. EVOH68−EVOH6 films were prepared by pressing the melts on a hot stage at temperatures 20 °C higher than their melting points and quenching into 15 °C. The film samples of EVOH100−EVOH52 were drawn by 5 times or higher the original lengths at 90 °C. The films of EVOH41−EVOH6 were drawn in a similar way at 60 °C. The drawn films were annealed by fixing the sample length in vacuo for 16 h. The annealing temperatures were 150 °C for EVOH100−EVOH90. The EVOH68−

* To whom correspondence should be addressed.
† Kuraray Co., Ltd.
‡ Osaka University.

10.1021/ma990521a CCC: $18.00
Published on Web 08/12/1999

Table 1. Unit Cell Dimensions and the Densities Obtained for a Series of EVOH Copolymers

sample	VA content (%)	a (Å)	b (Å)	γ (deg)	d_c[a] (g·cm^{-3})	d_o[a] (g·cm^{-3})
EVOH100	100	7.78	5.49	91.2	1.349	1.310
EVOH95	95	7.76	5.48	91.6	1.330	1.282
EVOH90	90	7.76	5.48	91.9	1.310	1.275
EVOH68	68	8.03	5.16	90.3	1.220	1.192
EVOH62	62	8.11	5.16	90.4	1.186	1.172
EVOH56	56	8.18	5.13	90.0	1.151	1.144
EVOH52	52	8.24	5.08	90.0	1.136	1.126
EVOH41	41	8.26	5.03	90.0	1.088	1.083
EVOH27	27	8.28	4.94	90.0	1.035	1.019
EVOH14	14	7.84	4.96	90.0	1.018	0.983
EVOH6	6	7.51	4.98	90.0	1.016	0.960
EVOH0	0	7.43	4.93	90.0	1.001	0.953

[a] d_o = observed density; d_c = calculated density.

Table 2. Fractional Coordinates of the Atoms in the Crystal Lattices of EVOH100∼Evoh27

sample	atom	x	y	z
EVOH100	C1	0.265	0.720	0.750
	C2	0.178	0.815	0.250
	O1	0.257	0.466	0.750
	O2	0.438	0.798	0.750
EVOH95	C1	0.268	0.722	0.750
	C2	0.181	0.817	0.250
	O1	0.258	0.466	0.750
	O2	0.441	0.799	0.750
EVOH90	C1	0.268	0.730	0.750
	C2	0.184	0.831	0.250
	O1	0.250	0.475	0.750
	O2	0.444	0.798	0.750
EVOH68	C1	0.271	0.736	0.750
	C2	0.189	0.845	0.250
	O1	0.254	0.469	0.750
	O2	0.440	0.801	0.750
EVOH62	C1	0.270	0.702	0.750
	C2	0.190	0.810	0.250
	O1	0.254	0.433	0.750
	O2	0.436	0.770	0.750
EVOH56	C1	0.271	0.706	0.750
	C2	0.198	0.826	0.250
	O1	0.240	0.438	0.750
	O2	0.440	0.749	0.750
EVOH52	C1	0.272	0.716	0.750
	C2	0.199	0.840	0.250
	O1	0.239	0.446	0.750
	O2	0.439	0.756	0.750
EVOH41	C1	0.270	0.716	0.750
	C2	0.209	0.856	0.250
	O1	0.215	0.454	0.750
	O2	0.440	0.718	0.750
EVOH27	C1	0.265	0.706	0.750
	C2	0.209	0.854	0.250
	O1	0.202	0.443	0.750
	O2	0.434	0.693	0.750

EVOH6 samples were annealed at temperatures 20 °C lower than their melting points. The thickness of the thus-obtained samples was about 0.6 mm.

Doubly oriented samples were prepared for EVOH90, EVOH68, and EVOH56 by rolling the uniaxially oriented samples at 100 °C along the drawn axes. The samples were annealed by sandwiching them between a pair of glasses in vacuo at the same temperatures as those used in the heat-treatment of the uniaxially drawn samples.

Thin films of 10−20 μm thickness were prepared for the measurements of FTIR spectra. The EVOH27 film was cast at 80 °C from the 10 wt % dimethyl sulfoxide solution. The EVOH16, EVOH6, and EVOH0 films were cast at 80 °C from 10 wt % *o*-dichlorobenzene solutions. These films were dried in vacuo at 80 °C for 1 day.

Measurements. The X-ray diffraction data were collected by using an X-ray imaging plate (IP) system (DIP1000, MAC Science Co. Ltd., Japan). Graphite-monochromatized Mo−Kα radiation was used as an X-ray source (50 kV, 200mA). The sample-to-IP distance was about 90 mm, which was calibrated by using Si powder as a standard. The thus-obtained X-ray diffraction data were transferred to a workstation in a digitized form. The fiber diagrams were transformed from the Cartesian coordinate system to the cylindrical coordinate system (ξ, ζ).[15] This transformation was made to convert the curved layer lines to the horizontal lines, making the data analysis easier. The data were corrected for the Lorentz and polarization factors. Evaluation of the integrated intensities and indexing of the observed reflections were performed by using software developed by Tashiro et al.[15] Indexing of the reflections and the determination of the cell parameters were carried out by a trial-and-error method by referring to the crystallographic data of PVOH and PE. The separation of the overlapped reflections was carried out by the method described in ref 15 and the integrated intensities of the thus-separated reflections were evaluated. The accidentally overlapped reflections were separated by taking into account the ratio of the structure factors calculated in the course of the least-squares refinement of the crystal structure.[15]

The FTIR spectra were measured by a Shimazu FTIR-8200PC spectrometer at a resolution of 1 cm^{-1}.

The densities of the samples were measured by a flotation method (hexane−carbon tetrachloride system) at 25 °C.

The DSC thermograms were measured by using a Perkin-Elmer DSC7 differential scanning calorimeter at a heating rate of 10 °C/min.

Table 3. *R* Factor and the Structural Data of EVOH with VA Content 100∼27 mol %

sample	N[a]	R factor (%)	θ[b] (deg)	B(C)[c] (Å^2)	B(O)[c] (Å^2)
EVOH100	24	17.2	36.8	7	6
EVOH95	25	19.5	37.0	6	3
EVOH90	25	13.9	39.3	8	5
EVOH68	20	14.7	40.8	14	8
EVOH62	16	16.4	40.1	12	5
EVOH56	14	12.3	45.6	13	3
EVOH52	12 (9[d])	2.5[e]	46.3	15	4
EVOH41	7 (5[d])	3.1[e]	54.4	19	12
EVOH27	7 (4[d])	2.7[e]	57.3	25	8

[a] Number of the observed reflections. [b] Setting angle of the planar-zigzag chain measured from the *a* axis (see Figure 6). [c] Isotropic temperature factors of C and O atoms. [d] Number of the observed equatorial reflections. [e] Calculated only for the equatorial reflections.

Table 4. Fractional Coordinates of the Atoms in the Crystal Lattices of EVOH14 and EVOH6

sample	atom	x	y	z
EVOH14	C1	−0.045	0.052	0.250
	O1	−0.214	−0.037	0.250
	O2	−0.042	0.333	0.250
EVOH6	C1	−0.044	0.056	0.250
	O1	−0.224	−0.017	0.250
	O2	−0.030	0.337	0.250

Table 5. *R* Factor and the Structural Data of EVOH with VA Content 14 and 6

sample	N[a]	R factor	θ[b] (deg)	B(C)[c] (Å)	B(O)[c] (Å)
EVOH14	10 (6[d])	5.9[e]	36.3	23	5
EVOH6	30	22.3	39.7	9	5

[a] Number of the observed reflections. [b] Setting angle of the planar-zigzag chain measured from the *a* axis (see Figure 6). [c] Isotropic temperature factors of C and O atoms. [d] Number of the observed equatorial reflections. [e] Calculated only for the equatorial reflections small.

Results and Discussion

X-ray Analysis. The X-ray fiber diagrams taken for the uniaxially oriented EVOH90, EVOH68, EVOH56,

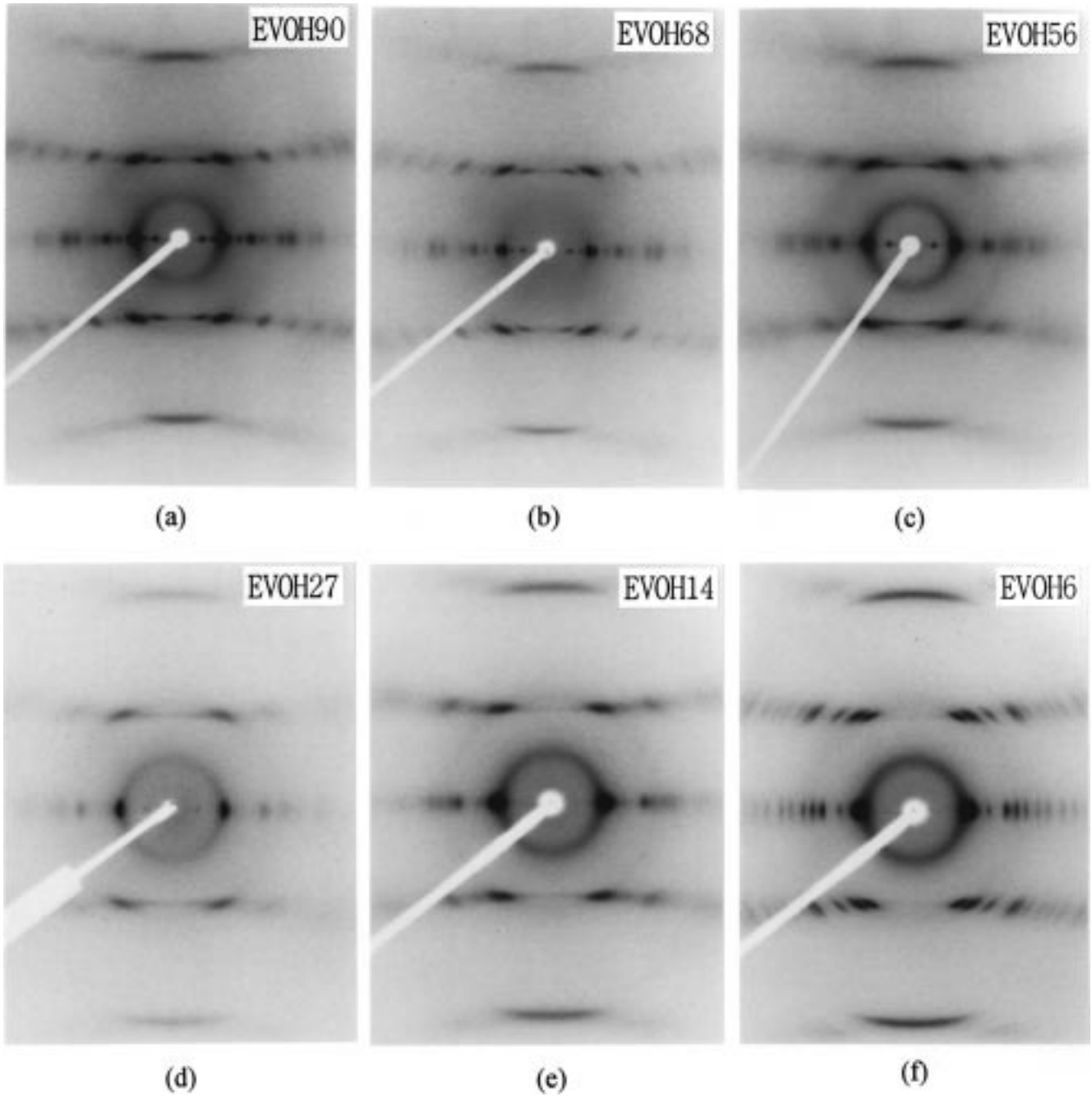

Figure 1. X-ray fiber diagrams. (a) EVOH90; (b) EVOH68; (c) EVOH56; (d) EVOH27; (e) EVOH14; (f) EVOH6. The vertical axes are along the fiber axes.

EVOH27, EVOH14, and EVOH6 samples are shown in Figure 1, where the drawn axes of the samples are vertical in the photographs. The fiber axis was assigned to the *c* axis. The *c*-axis length was evaluated from the interlayer distances. The fiber periods of all the EVOH samples were found to be essentially the same as those of PVOH and PE within experimental error, 2.54 Å, which corresponds to the fiber period of the planar-zigzag conformation. As already clarified,[2] the OH groups of atactic PVOH are arranged randomly on the right and left sides of the zigzag plane at a statistical weight of $^1/_2$. According to the NMR data, configurations of the EVOH copolymers are atactic and the VA and ET monomeric units are linked randomly along the EVOH chain.[16] In the X-ray fiber diagrams of a series of EVOH samples, any additional layer lines were not observed between the equatorial and the first-layer lines which were expected for the structures with a longer fiber period than 2.54 Å. This indicates that the EVOH chains take the statistically random array of VA and ET monomeric units along the planar-zigzag-type skeletal chains.

The observed X-ray reflections could also be indexed reasonably by assuming a random arrangement of the VA and ET segments in the common unit cell. By referring to the crystal structure of PVOH, the unit cells of all the EVOH members were found to be monoclinic or orthorhombic. The unit cell dimensions a, b, c, and γ, the densities calculated for the crystalline region (d_c) and the observed densities of the bulk sample (d_o) are given in Table 1. The VA content dependence of the unit cell dimensions a and b is shown in Figure 2. The densities calculated for the crystalline region and those observed for the bulk samples are shown in Figure 3.

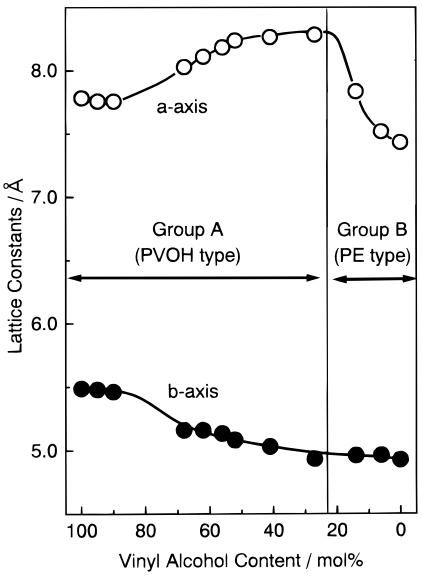

Figure 2. VA content dependence of the unit cell dimensions of EVOH samples. (a) *a*-axis length; (b) *b*-axis length.

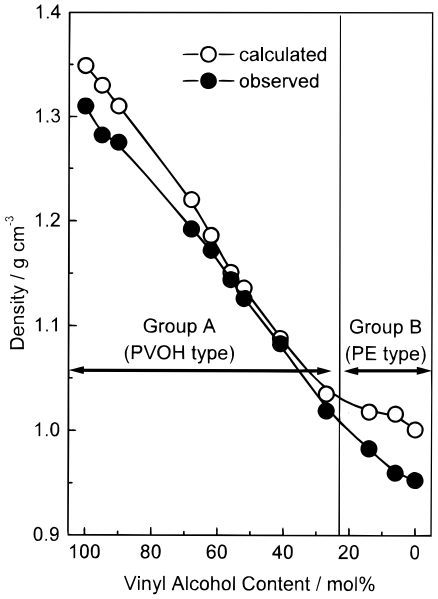

Figure 3. VA content dependence of the calculated and observed densities of EVOH samples.

The calculated and observed densities are relatively close to each other, indicating a high crystallinity of the EVOH copolymers despite random arrangements of the monomeric units in the crystal lattices. The VA content dependence of the melting point is shown in Figure 4.

As indicated in Figures 2−4, the series of EVOH copolymers may be classified into two groups, judging from the X-ray reflection patterns and the dependence of the lattice parameters, melting points and densities on the copolymer composition; group A covers the range of EVOH100−EVOH27 and group B is in the range of EVOH14−EVOH6. Group A is assumed to behave similarly to PVOH, while group B is of the PE type. The space group $P112_1/m$ was assumed for group A and the space group *Pnam* was assumed for group B. These assumptions were found reasonable as described in a later section.

The crystal structure model of the PVOH type is shown in Figure 5. The OH groups are set on the mirror planes perpendicular to the chain axis at the heights

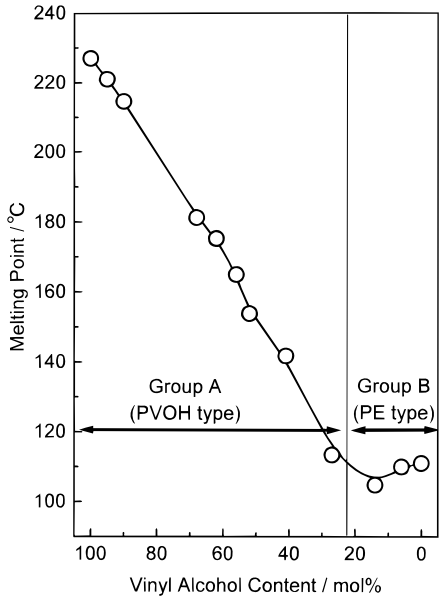

Figure 4. VA content dependence of the melting points of EVOH samples.

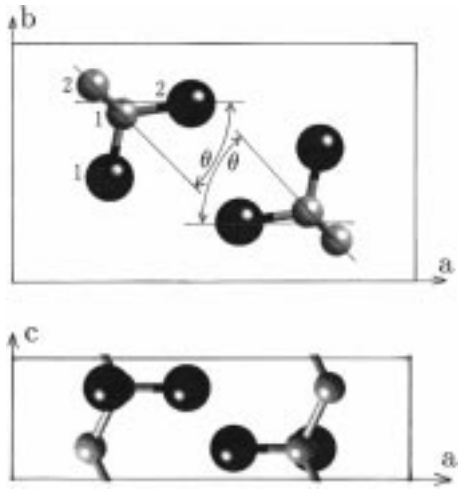

Figure 5. Crystal structure models of EVOH100∼EVOH27.

$^1/_4$ and $^3/_4$ and are arranged randomly on the right and left sides of the planar-zigzag chains. An averaged occupancy of the OH groups at one site is given by ($^1/_2$) × (VA content). When the two zigzag chains are packed in the cell, 2 degrees of freedom are assumed: the first one is an interchain distance in the *ab* plane and the second one is a setting angle (θ) of the chains which is defined as an angle between the *a* axis and the C−C zigzag plane (Figure 5). In addition to these two variables, the isotropic temperature factors of the C and O atoms and the scale factor between the observed and calculated reflection intensities were used as the adjustable parameters for the crystal structure refinement. The molecular chains were assumed to be rigid: The bond distances were fixed to 1.531 Å for the C−C bond and 1.398 Å for the C−O bond. The bond angles were ∠C−C−C 111.0°, ∠O−C−O 109.3°, and ∠C−C−O 109.4°.

The crystal structure model of the PE type is shown in Figure 6. The OH groups were assumed to be attached apparently to all the carbon atoms with equal weights from the requirement of space group symmetry. Therefore, the fraction of the OH groups at one carbon atom is ($^1/_4$) × (VA content). Because the chain has the direction −CH−CH(OH)− along the *c* axis, the upward

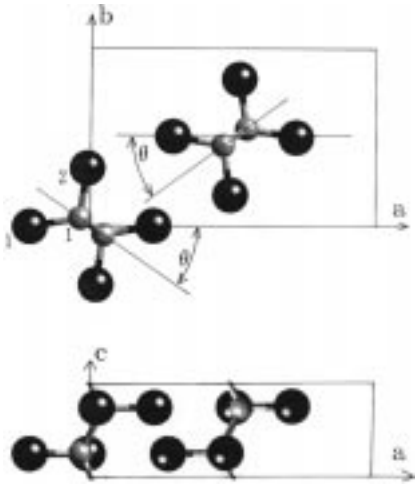

Figure 6. Crystal structure models of EVOH14 and EVOH6.

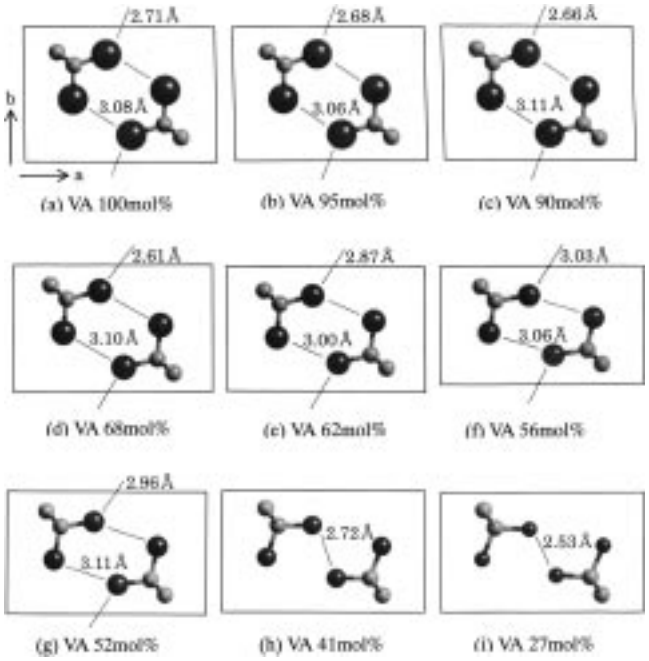

Figure 7. Crystal structures of EVOH100∼EVOH27. The existence weights of oxygen atoms are represented by the sizes of the corresponding balls.

and the downward chains were assumed to be located at the same site at the same probability. The packing of the two chains is represented by a setting angle (θ) of the chains or an angle between the *a* axis and the C−C zigzag plane (Figure 6). The intramolecular geometry of the chain is essentially the same as that of the PVOH-type model.

The least-squares refinement of the structural models was carried out by the quantitative comparison of the calculated structural factors $|F_{calc}(hkl)|$ with the observed ones $|F_{obs}(hkl)|$. The reasonability of the thus-obtained structure was evaluated by using the following reliability factor (*R* factor):

$$R \text{ factor} = \frac{\sum||F(hkl)_{obs}| - |F(hkl)_{calc}||}{\sum|F(hkl)_{obs}|}$$

The structures of EVOH100−EVOH56 and EVOH 6 were refined by using all the reflections of the equatorial and layer lines. Different from these cases, the structures of EVOH52−EVOH14 were refined using only the equatorial reflections because only a few diffuse X-ray reflections were observed on the first layer and therefore the exact evaluation of the intensity of layer-line reflections was difficult. The temperature factor of the oxygen atom was determined to be ca. 5 Å^2 for EVOH100−

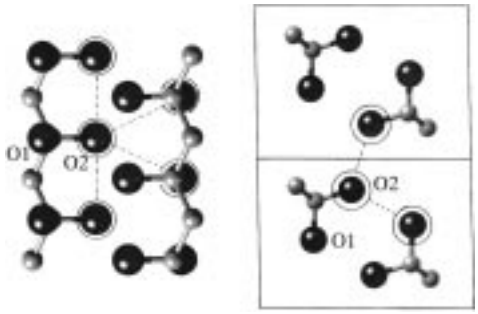

Figure 8. An illustration of pairs of O2 groups forming hydrogen bonds.

Table 6[a]

	EVOH100		EVOH94.8		EVOH90	
hkl	$\|F_{obs}(hkl)\|$	$\|F_{calc}(hkl)\|$	$\|F_{obs}(hkl)\|$	$\|F_{calc}(hkl)\|$	$\|F_{obs}(hkl)\|$	$\|F_{calc}(hkl)\|$
100	2.6	2.8	1.9	2.5	2.3	2.6
010	1.6	1.9	1.2	1.4	1.0	0.8
1$\bar{1}$0	10.1	9.6	8.7	8.3	9.8	9.3
110	9.9	9.4	8.5	8.1	9.5	9.0
200	7.7	7.8	6.7	6.8	7.5	7.5
2$\bar{1}$0	2.0	3.2	1.3	2.8	1.5	2.8
210	1.9	3.0	1.1	2.5	1.4	2.1
020	4.9	4.3	3.8	3.8	3.3	3.7
1$\bar{2}$0					0.9	1.0
300	1.6	2.3	1.2	2.0	2.2	2.4
120	2.0	3.0	1.6	2.8	3.1	3.5
310	1.7	2.1	1.7	2.1	1.8	2.2
2$\bar{2}$0					0.4	0.7
220					0.5	0.9
400	3.3	2.4	4.2	2.5	3.3	2.7
030			2.6	2.5	2.9	2.8
410	3.1	3.4	3.4	3.2	3.1	2.9
1$\bar{3}$0	2.5	2.8	2.9	2.7	2.4	2.3
130	2.3	2.5	2.5	2.3	1.9	1.8
4$\bar{2}$0					1.1	1.4
420	0.8	1.6	1.2	1.6	1.3	1.7
330	1.6	2.3	2.4	2.4	2.0	2.0
510	1.0	1.5	1.7	1.7	1.5	1.5
230					1.2	1.2
040			0.9	1.3	1.2	1.1
101	2.3	2.8	1.6	2.5	1.8	2.5
1$\bar{1}$1	7.7	4.9	7.5	4.6	6.7	4.8
201	4.2	3.1	4.6	2.9	4.2	2.7
211	0.9	1.1	0.7	1.1	0.9	1.3
3$\bar{1}$1	3.1	2.9	3.4	2.9	2.5	2.7
2$\bar{2}$1	2.8	2.6	3.1	2.6	2.6	2.4
031	1.4	1.4	1.6	1.6	1.6	1.7
411	1.1	1.1	1.1	1.1	0.7	0.7
1$\bar{3}$1	1.3	1.3	1.3	1.3	0.8	0.8
401			0.5	1.0		
501	2.5	2.3	2.5	2.6	2.2	2.2
5$\bar{1}$1			1.2	1.2	1.1	1.1
041	1.1	1.0	0.8	1.0		
5$\bar{2}$1	1.0	0.9	0.8	1.0	0.7	0.7
141	1.5	1.4	1.4	1.8	1.6	1.7
2$\bar{4}$1	1.8	1.4	2.1	1.8	1.5	1.2
601	1.2	0.9	1.5	1.3	1.2	0.9
241	1.4	1.1	1.5	1.3	1.3	1.0
6$\bar{1}$1	1.3	1.0	1.3	1.1	1.2	1.0
611	1.3	1.0	1.2	1.0	0.7	0.5
621	0.9	0.8				
022	0.9	0.8	0.9	0.9		

[a] The sum of the observed reflections and the sum of the calculated reflecions were set to 100.

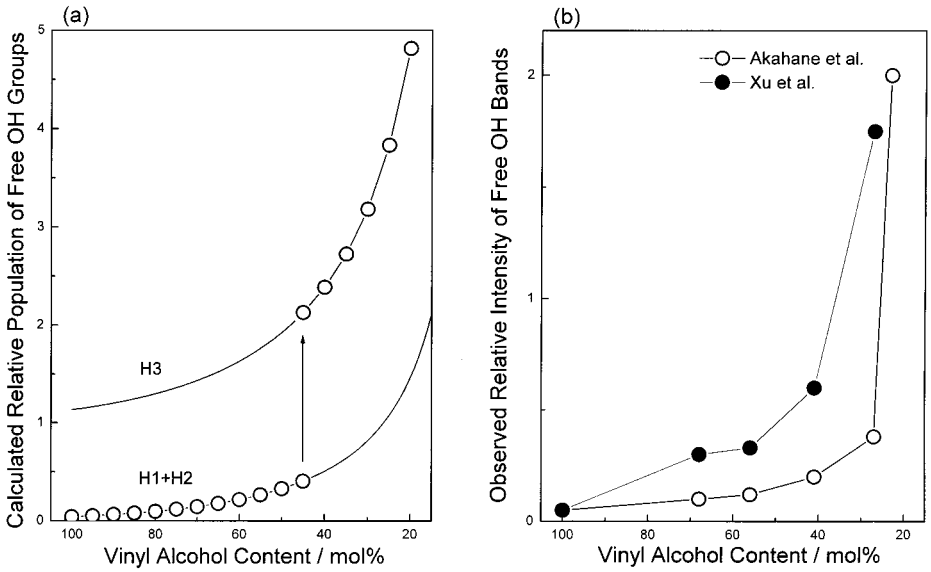

Figure 9. VA content dependence of the relative population of free OH groups. (a) Calculated relative population of free OH groups; (b) observed relative intensity of free OH bands.

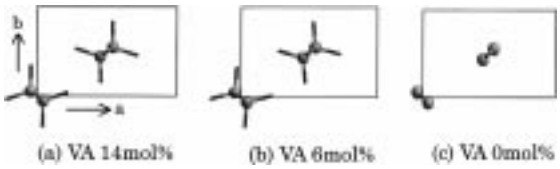

Figure 10. Crystal structures of EVOH14∼EVOH0. The existence weights of oxygen atoms are represented by the sizes of the corresponding balls.

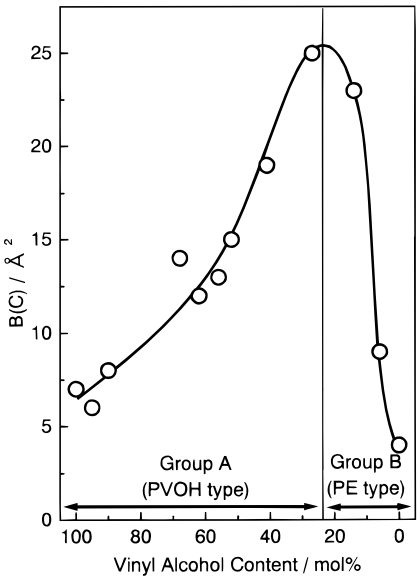

Figure 11. VA content dependence of temperature factors of carbon atoms.

EVOH27. This value was applied also to the cases of EVOH14 and EVOH6 because the presence probability of oxygen atoms was too low to determine the temperature factors. The standard deviations were estimated to be about $^1/_{200}$ for all the cases.

Group A: The thus-determined atomic fractional coordinates of EVOH100−EVOH27 are shown in Table 2. The corresponding *R* factor, the setting angle (θ), and the temperature factor are shown in Table 3. The calculated and observed structure factors of EVOH100−EVOH90 are shown in Appendix A. Those of EVOH68−EVOH56 and EVOH52−EVOH27 are shown in Appendices B and C, respectively.

Group B: The obtained atomic fractional coordinates of EVOH14 and EVOH6 are shown in Table 4. The corresponding *R* factor, the setting angle (θ), and the temperature factor are shown in Table 5. The calculated and observed structure factors of EVOH14 and EVOH6 are shown in Appendices D and E, respectively.

For both groups A and B, the calculated structure factors agree relatively well with the observed structure factors as seen in the appendices. The determined crystal structure of EVOH100 or poly(vinyl alcohol) is essentially the same as the reported structure.[2]

Detailed Description of the Analyzed Crystal Structures. Densities of the crystalline region (d_c) are higher than those of the bulk samples (d_o) by 10−20% for all the EVOH copolymers as seen in Figure 3. Both the d_c and d_o change continuously depending on the VA content, suggesting the reasonability of the assumption that the VA content in the crystal lattice is essentially equal to that of the bulk sample.

The melting point changes continuously depending on the VA content, as shown in Figure 4. With a decrease in VA content, the melting point decreases in group A while it increases in group B.

The lattice constants also change continuously depending on the VA content, as shown in Figure 2. With a decrease in VA content from EVOH100, the crystal system changes from monoclinic of PVOH to hexagonal. For example, the ratio a/b calculated for EVOH27 is 1.66, which is close to the value $a/b = 1.73$ expected for the hexagonal system. The lattice constants change rapidly between EVOH27 [group A] and EVOH14 [group B]. The unit cell of EVOH14 approaches that of PE as the VA content decreases furthermore. The crystal structures of EVOH are consisted of the statistically disordered packing of VA and ET units. The OH groups are arranged on the right and left sides of the zigzag planes. The orderliness of the crystal structure is considered to be low for the samples located in the transition region between groups A and B. In fact, the number of the observed X-ray reflections decreases in group A with a decrease in VA content, while it increases in group B from EVOH14 to EVOH6. We

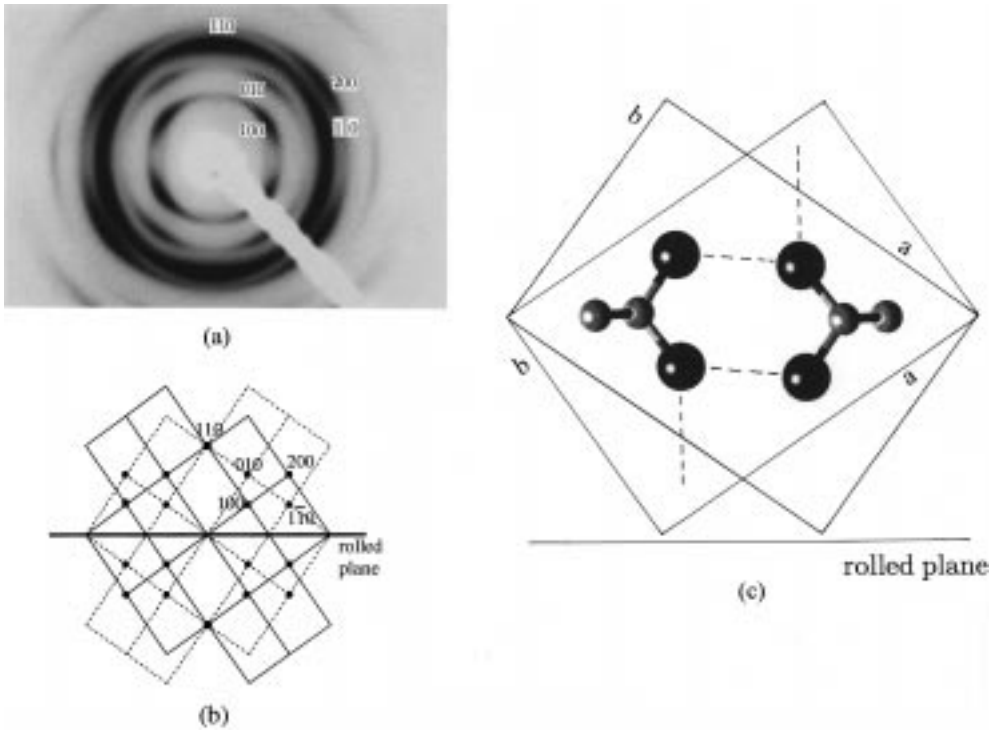

Figure 12. (a) X-ray photograph taken along the end direction (the draw direction) of the doubly oriented sample of EVOH90. The rolled plane is horizontal in this photograph; (b) indexing of the observed reflections on the reciprocal lattice plane a^* b^*; (c) the relationship of the rolled plane with the unit cell structure.

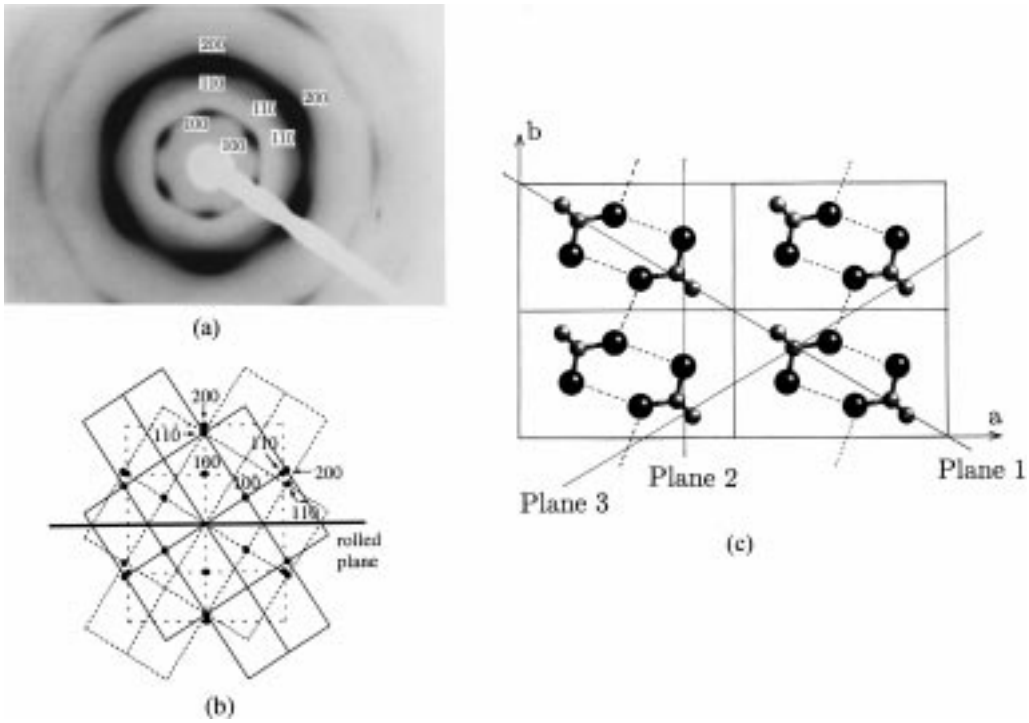

Figure 13. (a) X-ray photograph taken along the end direction (the draw direction) of the doubly oriented sample of EVOH56. The rolled plane is horizontal in this photograph; (b) indexing of the observed reflections on the reciprocal lattice plane a^* b^*; (c) the relationship of the rolled plane with the unit cell structure.

might also expect the diffuse scatterings coming from the statistically disordered packing structure, but they could not be detected in the X-ray fiber diagrams of all the EVOH samples.

Group A. As shown in Figure 7, the packing mode of the chains changes with a decrease in VA content. The setting angle (θ) changes remarkably, depending on the VA content (Table 3). The θ becomes larger with a decrease in VA content. The C−C zigzag plane of EVOH100 in the unit cell is parallel to the (110) plane. This geometry is broken in the crystal of EVOH with lower VA content. The hydrogen bonds between the oxygen atoms are indicated by broken lines in Figure 7. Pairs of PVOH chains in one unit cell are connected by the hydrogen bonds of 3.08 Å (H1). Also, these chains are connected along the *b* axis by another type of

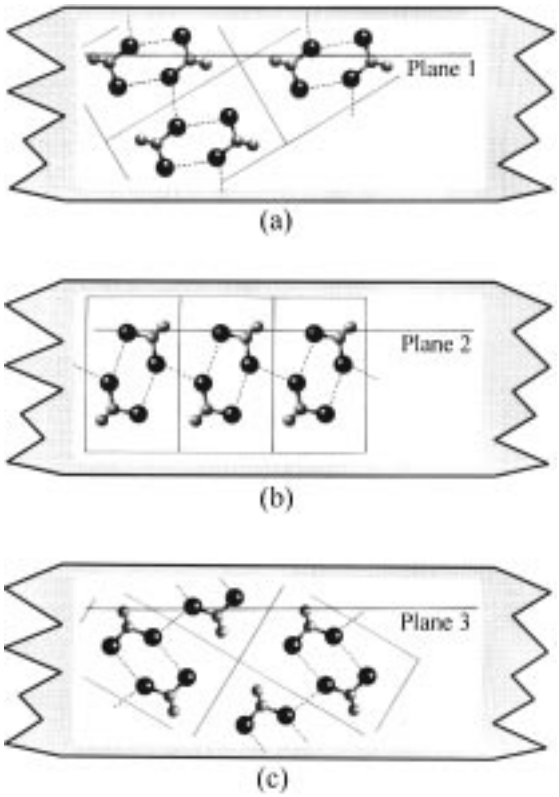

Figure 14. Orientation of crystallites in the doubly oriented samples of EVOH56. (a) Along plane 1; (b) along plane 2; (c) along plane 3 (refer to Figure 13).

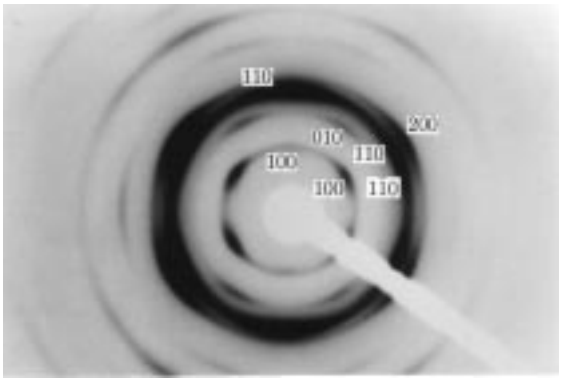

Figure 15. X-ray photograph taken along the end direction of the doubly oriented sample of EVOH68. The rolled plane is horizontal in the photograph.

intermolecular hydrogen bonds of 2.71 Å (H2), forming a kind of sheet structure along the *b* axis. Despite the atactic configuration, the H1 and H2 hydrogen bonds are formed efficiently and only few OH groups are free in the unit cell of PVOH. In the EVOH cases, the setting angle changes and this hydrogen-bonding system of PVOH is deformed more or less. Although the change is slight and the experimental error also needs to be considered, the hydrogen bond H1 tends to become longer for the samples with a VA content lower than 52 mol %. The H2 becomes longer for VA content lower than 56 mol %. In the EVOH sample with low VA content, another type of hydrogen bond (H3) is formed as shown in Figure 7h,i. Many free OH groups are expected for these EVOH samples because of the difficulty to form hydrogen bonds of the H1 and H2 types. The population of free OH groups can be evaluated roughly in the following two cases. The first one is the

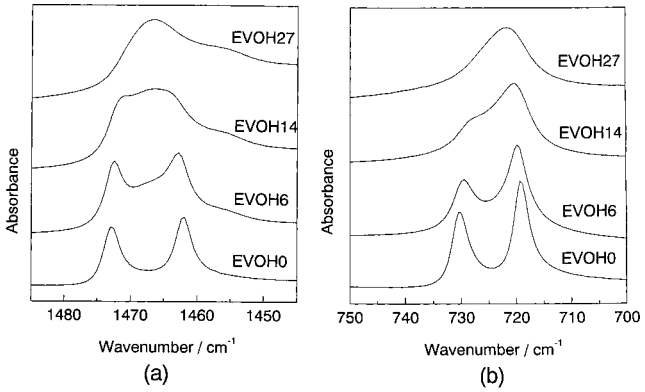

Figure 16. IR spectra of unoriented EVOH samples with VA = 0, 6, 14, and 27 mol %.

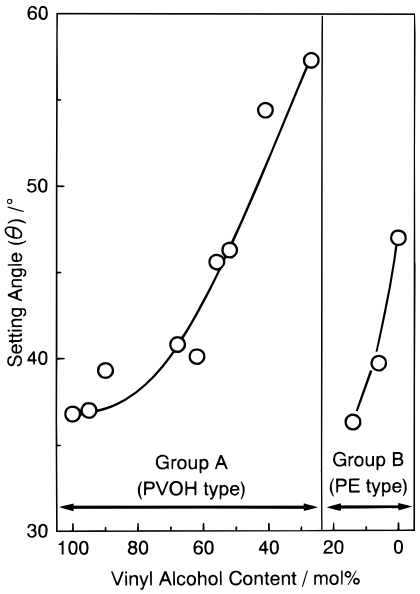

Figure 17. VA content dependence of the setting angle (θ) of the EVOH chains (refer to Figures 5 and 6).

case where the H1 and H2 hydrogen bonds are formed (case H1 + H2), and the second one is the case where the H3 hydrogen bond is formed (case H3).

Case H1 + H2: Existence weights w_{OH} of the O1 and O2 hydroxy groups as the side groups are equal to each other, 0.5, if the statistically random conformation is assumed for the chains. When the ethylene units are introduced into the PVOH chain, the probability that the neighboring substituent is not an OH group is $1 - w_{OH}X_{VA} = 1 - X_{VA}/2$, where X_{VA} is the VA content. The O2 group is surrounded by six OH substituents as shown in Figure 8, where the circumstances of one OH group (O2) are shown from the various directions. Therefore the probability that the O2 has no OH groups as neighbors is $(^1/_2)(1 - X_{VA}/2)$.[6] In the same manner, the probability that the O1 group has no neighboring OH groups is $(^1/_2)(1 - X_{VA}/2)$.[4] As a result, the total probability to possess the free OH groups is $(^1/_2)(1 - X_{VA}/2)^4 + (^1/_2)(1 - X_{VA}/2)$.[6]

Case H3: The probability that an OH group does not form any hydrogen bond is calculated to be $(^1/_2)(1 - X_{VA}/2)^4 + {}^1/_2$.

The calculated relative populations of the free OH groups of the above-mentioned two cases are shown in Figure 9a. When we apply these calculated curves to the actual cases, we have to consider that the hydrogen-

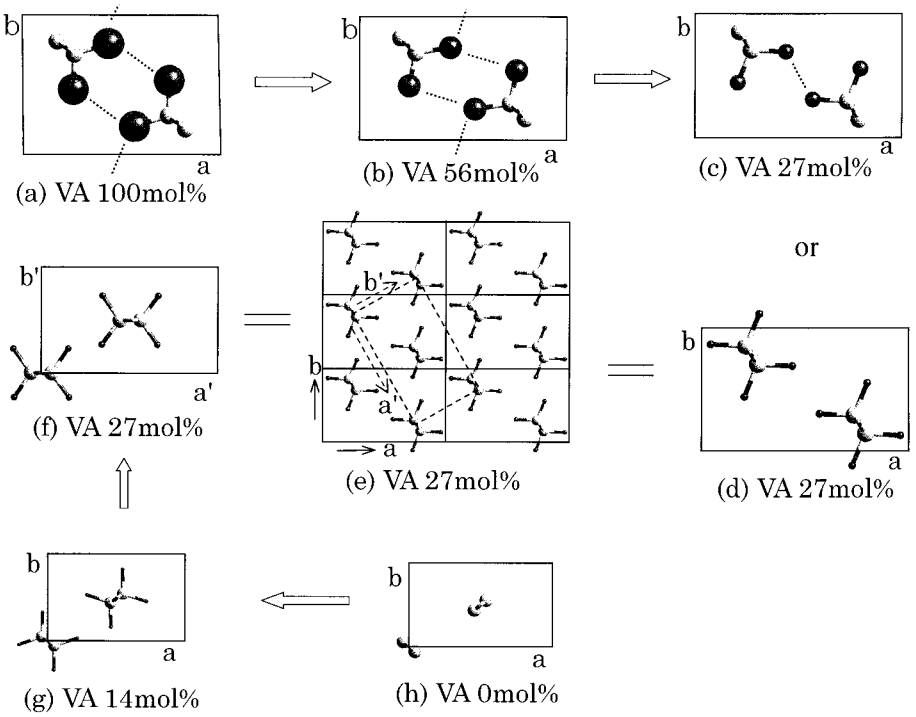

Figure 18. Illustration of the transformation of the crystal structure of EVOH samples with different VA content. The structure of the EVOH27 sample can be assumed as either (c) and (d) (refer to the text).

bonding mode changes depending on the VA content, as indicated in the previous section. That is, the observed curve must be compared with the calculated curve H1 + H2 in the VA content of 100−52 mol % and with the curve H3 in the VA content of 41−27 mol %. Akahane et al. measured the near-IR spectra for a series of EVOH samples and evaluated the relative intensity of the IR bands of free OH groups as $I = A_{free}/(A_{free} + A_{bonded})$, where A_{free} is an absorbance of the O−H stretching band of the free OH groups and A_{bonded} is that for the hydrogen-bonded OH groups.[17] Xu et al. reported a similar result by measuring the IR band intensities of the C−O stretching modes.[18] The relative intensities of free OH bands reported by Akahane et al. and Xu et al. are shown in Figure 9b. According to their results, the relative amount of free OH groups increases steeply in the vicinity in the VA content of ca. 50 mol %. By comparing Figure 9a with 9b, we may say the calculated curve corresponds to the observed curve, indicating that the steep change of the observed IR intensity ratio originates from the drastic structural change between the monoclinic (H1 + H2) type and hexagonal (H3) type.

Group B. The crystal structures of EVOH14 and EVOH6 are shown in Figure 10. The setting angle (θ) of the chain is close to that of orthorhombic PE.

Temperature Factors. VA content dependence of the temperature factors of the carbon atom [B(C)] is shown in Figure 11. In group A, the B(C) tends to become larger with a decrease in VA content and is maximal at EVOH27. B(C) becomes smaller again with a further decrease in VA content. This behavior of the temperature factor is similar with the change in the lattice constants (Figure 2). An increase of the temperature factors is accelerated as the crystal lattice approaches the hexagonal type. The temperature factor determined in the structure analysis is contributed apparently not only by the thermal motion of the atoms but also by the structural irregularity such as lattice strain, etc. Therefore, the increase of the temperature factor is considered to reflect the increasing disorder of the chain-packing structure as well as the increasing thermal behavior.

Double Orientation. The X-ray diffraction pattern of the doubly oriented EVOH90 sample is shown in Figure 12a where the X-ray beam was incident along the chain axis. Indexing of the X-ray reflections is shown in Figure 12b. The (110) planes orient parallel to the rolled plane, and the unit cells orient into two possible directions by sharing the (110) plane or the twin structure [Figure 12c]. All these features are similar to those observed for PVOH.[19]

The double orientation of EVOH56 shown in Figure 13a is clearly different from that of EVOH90 shown in Figure 12a. Indexing of the X-ray reflections is shown in Figure 13b. Three types of orientations were possible as shown in Figure 13c, indicating that the planes 1, 2, and 3 can become parallel along the rolled plane, as shown in Figure 14. The planes which give the compact atomic arrangement may tend to be parallel to the rolled plane. X-ray scattering intensities of the three 100 reflections shown in Figure 13a are approximately the same and the possibility of the plane being parallel to the rolled plane is almost the same. That is to say, the fractions of the microcrystallites shown in Figure 14 a−c are considered almost the same. Another assumption may be possible that the C−C zigzag planes are statistically randomly oriented along the planes 1, 2, and 3 in one unit cell. But the structure factors calculated for such a model did not agree with the observed data at all.

The X-ray diagram of the doubly oriented sample of EVOH68 is shown in Figure 15. The 100 reflection appeared upward and downward in the X-ray photograph like that in EVOH56. The model shown in Figure 14b is considered to be applicable to this case. But the intensities of these 100 reflections are relatively week compared with those of 110 reflections, suggesting that the probability of the presence of microcrystallites shown in Figure 14b is low. The EVOH52, EVOH41,

Table 7[a]

	EVOH68		EVOH62		EVOH56	
hkl	$\|F_{obs}(hkl)\|$	$\|F_{calc}(hkl)\|$	$\|F_{obs}(hkl)\|$	$\|F_{calc}(hkl)\|$	$\|F_{obs}(hkl)\|$	$\|F_{calc}(hkl)\|$
100	3.1	2.8	2.1	2.5	2.4	2.5
1$\bar{1}$0	13.0	12.2	13.2	13.1	13.5	13.5
110	13.9	12.9	14.9	14.8	16.0	16.1
200	9.9	11.3	13.4	13.4	14.5	14.5
2$\bar{1}$0	1.4	2.4				
210	0.9	1.5				
020	4.0	4.0	6.7	6.5	7.1	6.2
1$\bar{2}$0	1.8	1.8				
300	2.5	2.5				
120	4.5	4.5				
310	2.0	3.3	2.7	3.1	3.2	3.1
220	1.2	1.4	1.4	2.6	2.3	2.8
400	3.1	3.0	3.7	3.8	4.2	4.6
410	2.4	2.7	3.1	4.2	3.5	3.9
0$\bar{3}$0	3.3	2.4	0.8	1.0		
1$\bar{3}$0	2.4	1.8	2.2	2.8	1.8	2.3
130	1.8	1.4	2.6	3.4	2.9	3.7
4$\bar{2}$0	1.0	1.2				
230	1.1	1.3				
420	1.3	1.6			1.6	2.0
510	1.3	1.6	1.5	1.9	1.6	2.0
101	1.7	2.6	1.1	3.1	0.8	3.2
1$\bar{1}$1	5.9	5.0	9.2	6.2	10.0	6.9
201	3.8	3.1	5.7	3.8	5.1	3.5
211	0.9	1.3				
3$\bar{1}$1	3.3	2.6	4.2	3.6	4.0	3.6
2$\bar{2}$1	2.5	2.0	2.9	2.8	2.6	2.6
401	1.2	0.8				
031	1.5	1.4	0.7	1.7		
501	1.5	1.6				
2$\bar{3}$1	1.2	1.3	1.4	1.0	0.9	0.8
5$\bar{1}$1	0.7	0.8	2.0	1.4	2.0	1.8
601			1.5	1.1		
6$\bar{1}$1			1.0	0.7		
4$\bar{3}$1			1.0	0.8		
431			0.9	0.7		

[a] The sum of the observed reflections and the sum of the calculated reflecions were set to 100.

Table 8[a]

	EVOH52		EVOH41		EVOH27	
hkl	$\|F_{obs}(hkl)\|$	$\|F_{calc}(hkl)\|$	$\|F_{obs}(hkl)\|$	$\|F_{calc}(hkl)\|$	$\|F_{obs}(hkl)\|$	$\|F_{calc}(hkl)\|$
100	3.0	3.2	2.1	2.1	0.8	0.8
1$\bar{1}$0	18.7	18.6	19.9	20.0	21.4	21.4
110	22.1	22.0	24.4	24.4	26.7	26.7
200	20.3	20.2	22.8	22.8	25.3	25.3
0$\bar{2}$0	7.9	7.2	6.1	5.8	5.3	4.9
3$\bar{1}$0			3.7	3.5	4.1	3.8
310	4.5	4.6	5.9	5.6	5.3	5.0
220	2.8	3.2	3.8	4.3	3.8	4.3
400	5.9	5.7	4.5	5.1	3.6	4.1
410	3.8	4.3	1.4	1.6	1.3	1.5
1$\bar{3}$0	2.4	2.4	0.5	0.4		
130	3.6	3.6	2.6	2.2	2.5	2.1
420	2.6	2.4				
510	2.6	2.4	2.4	2.0		
1$\bar{1}$1	m	8.4	m	6.9	m	6.4
201		4.3		2.9		2.3
3$\bar{1}$1	w	4.2	w	3.1	w	2.2
2$\bar{2}$1	w	3.0		2.4		1.5

[a] The sum of the observed zero-layer's reflections and the sum of the calculated zero-layer's reflections were set to 100. The observed first-layer's reflections were indicated as medium (m) or weak (w).

and EVOH27 samples were found to show the double-orientation character similar to that of EVOH56.

IR Spectra. The IR spectra observed for EVOH27−EVOH0 are shown in Figure 16. A pair of bands at 719 and 731 cm^{-1} of EVOH0(PE) corresponds to the correlation splitting of the methylene rocking modes by intermolecular vibrational coupling. A pair of bands at 1462 and 1473 cm^{-1} are the splitting pair of methylene bending modes ($\delta(CH_2)$).[20] With an increase in VA content, the splitting width is smaller and the relative intensity of the 731-cm^{-1} band is weaker. These behaviors are similar to those observed in the phase transition of PE from the orthorhombic to hexagonal phase.[21] In other words, the correlation between the ethylene sequences of the neighboring chains becomes lower, resulting in the observed change of the IR band profile.

Table 9[a]

hkl	$\|F_{obs}(hkl)\|$	$\|F_{calc}(hkl)\|$	*hkl*	$\|F_{obs}(hkl)\|$	$\|F_{calc}(hkl)\|$
110	37.5	37.6	011		4.4
200	32.0	32.1	111	m	3.6
020	14.9	12.4	201		6.0
310	6.7	6.3	121	w	1.7
220	2.6	4.6	311		1.9
400	4.3	4.4	221	w	1.4
130	1.9	2.7	231	w	0.9
			131		0.7

[a] The sum of the observed zero-layer's reflections and the sum of the calculated zero-layer's reflections were set to 100. The observed first-layer's reflections were indicated as medium (m) or weak (w).

Table 10[a]

hkl	$\|F_{obs}(hkl)\|$	$\|F_{calc}(hkl)\|$	*hkl*	$\|F_{obs}(hkl)\|$	$\|F_{calc}(hkl)\|$
110	16.9	15.8	211	2.7	1.9
200	12.0	13.4	121	4.0	3.0
210	1.9	2.2	311	2.8	3.1
020	6.5	7.1	221	1.2	1.8
310	3.2	4.8	401	1.8	3.4
220	2.8	4.3	321	1.0	1.4
400	2.7	2.8	411	0.4	0.6
320	1.7	2.5	031	2.4	2.6
410	1.2	1.7	231	2.0	1.8
130	1.8	2.2	511	1.9	2.0
230	1.4	1.7	141	2.4	1.3
520	1.1	1.4	621	1.0	0.7
600	0.3	0.2	531	0.7	0.5
430	1.9	1.7	341	0.9	0.6
040	0.4	0.4	022	1.2	1.1
340	1.2	1.0	312	0.9	0.8
011	5.0	2.9	222	0.6	0.7
111	3.3	2.1	322	0.5	0.4
201	6.1	3.9	412	0.4	0.3

[a] The sum of observed reflections and the sum of the calculated reflections were set to 100.

Table 11[a]

hkl	$\|F_{obs}(hkl)\|$	$\|F_{calc}(hkl)\|$
100	0.8	0.8
1$\bar{1}$0	21.5	21.4
110	27.8	27.8
200	25.5	25.4
0$\bar{2}$0	6.9	6.9
3$\bar{1}$0	1.4	1.4
310	5.0	5.0
220	3.1	3.2
400	4.5	4.7
410	0.1	0.2
1$\bar{3}$0	2.3	2.1
1$\bar{1}$1	m	6.0
201		3.2
3$\bar{1}$1	w	1.9
2$\bar{2}$1		0.9

[a] The sum of the observed zero-layer's reflections and the sum of the calculated zero-layer's reflections were set to 100. The observed first-layer's reflections were indicated as medium (m) or weak (w).

As already pointed out in the previous sections, the EVOH27 takes the pseudohexagonal system, and the EVOH copolymers with lower VA content change to the structure of the orthorhombic PE type. The IR spectral change is consistent with this structural transition revealed by the X-ray analysis.

Crystal Structure Change of EVOH. The setting angles θ of EVOH samples are shown in Figure 17. θ increases with a decrease in VA content in group A. This tendency is seen also in group B: the θ decreases with an increase in VA content. The crystal structure change deduced from the behavior of θ is illustrated in Figure 18 where the structures of (d−f) are not actually found. In group A, the crystal structure changes from (a) to (c) as the VA content is decreased. Because the OH groups can be located randomly at the various carbon atoms in such a case of low VA content, then another model, (d), is also possible for the crystal structure of the VA 27 mol % sample. This model, (d), can give a similar X-ray scattering pattern to the model (c) because the contribution of the O atoms to the scattering intensity is relatively low. The indexing of the lattice plane and the structure factors calculated for the two types of structures taken for the EVOH27 sample are compared between Appendices C and F. As a whole, the calculated and observed intensities are relatively in good agreement for both models. This result is important. The X-ray diffraction data of the VA 27 mol % sample can be interpreted in the two ways of monoclinic and hexagonal unit cells. Therefore, we cannot say which model is more proper for the VA 27 mol % sample. In other words, we might assume the coexistence of the structures (c) and (d) for the samples with the VA content close to 27 mol %, where the preferability to take the model (c) or (d) depends sensitively on the VA content. That is, VA content of ca. 27 mol % may be a boundary in the structure transition between groups A and B. If we accept model (d) for the VA 27 mol % sample, then we can take another type of unit cell as shown by broken line in model (e). The structure shown by the broken line is equivalent to model (f) with the unit cell parameters a' and b', which is the unit cell of the orthorhombic type. Figure 18h is the crystal structure of EVOH0(PE) and Figure 18g is that of EVOH14. The setting angle θ tends to decrease with an increase in VA content in group B. If the θ decreases furthermore and approaches zero, then the crystal structure results in that shown in Figure 18f, which is just equal to the structure (e) or (d). In this way, the packing mode of chains can change gradually and continuously by introducing the ethylene unit into the PVOH chain. To confirm the reasonability of this structural transformation model shown in Figure 18, an existence of the structure model (e) must be checked. More concretely, a structural change from model (g) to model (f) is needed to be checked. For example, the structure analysis of the sample with a VA content of ca. 20 mol % is required, although it has not yet been made because of a lack of a corresponding sample.

Conclusions

The crystal structure was determined for a series of ethylene−vinyl alcohol copolymers (EVOH). It was revealed that all the EVOH samples can crystallize and the crystal structure changes continuously with change in the copolymer composition. Such a continuous structural change is considered to come from the statistically disordered packing structure which consisted of a random arrangement of ethylene and vinyl alcohol units. EVOH samples with 100−27 mol % VA content take the structure of the poly(vinyl alcohol) (PVOH) type and approach the hexagonal structure with a decrease in VA content. EVOH samples with 14−6 mol % VA content show the crystal structure of the polyethylene (PE) type. A boundary of crystal structure transformation between the PVOH type and PE type is considered to be located at a VA content between 27 and 14 mol % because the X-ray pattern can be interpreted almost equally on the basis of both the PVOH- and PE-type structure models. The continuous structural change between PVOH- and PE-type structures may be caused by a continuous change of the setting angle of the zigzag chains as shown in Figure 18. Computer simulation might be useful to confirm this speculative structure change.

Acknowledgment. The authors wish to thank Mr. Makio Tokoo of the EVAL Laboratory of Kuraray Co., Ltd., for supplying the samples.

Appendix A

Table 6 shows a comparison between the observed and calculated intensities of different reflections of EVOH100, EVOH95, and EVOH90.

Appendix B

Table 7 shows a comparison between the observed and calculated intensities of different reflections of EVOH68, EVOH62, and EVOH56.

Appendix C

Table 8 shows a comparison between the observed and calculated intensities of different reflections of EVOH52, EVOH41, and EVOH27.

Appendix D

Table 9 shows a comparison between the observed and calculated intensities of different reflections of EVOH14.

Appendix E

Table 10 shows a comparison between the observed and calculated intensities of different reflections of EVOH6.

Appendix F

Table 11 shows a comparison between the observed and calculated intensities of different reflections of the model (d) shown in Figure 18.

References and Notes

(1) Foster, R. H. *Modern Plastics Mid-October Encyclopedia Issue*; McGraw-Hill: New York, 1990, Vol. 67, p 73.
(2) Bunn, C. W. *Nature* **1948**, *161*, 929.
(3) Bunn, C. W. *Trans. Faraday Soc.* **1939**, *35*, 482.
(4) Swan, P. R. *J. Polym. Sci.* **1962**, *56*, 409.
(5) Tashiro, K.; Ishino, K.; Ohta, T. *Polymer* **1999**, *40*, 3469.
(6) Seto, T.; Hara, T.; Tanaka, K. *Jpn. J. Appl. Phys.* **1968**, *7*, 31.
(7) Bassett, D. C.; Block, S.; Piermarini, G. J. *J. Appl. Phys.* **1974**, *45*, 4146.
(8) Yasuniwa, M.; Enoshita, R.; Takemura, T. *Jpn. Appl. Phys.* **1976**, *15*, 1421.
(9) Yamamoto, T.; Miyaji, H.; Asai, K. *Jpn. J. Appl. Phys.* **1977**, *16*, 1891.

(10) Tanaka, H.; Takemura, T. *Polym. J.* **1980**, *12*, 355.
(11) Akahane, K.; Mochizuki, R. *Koubunshi Kagaku* **1971**, *28*, 577.
(12) Matsumoto, T.; Nakamae, K.; Ogoshi, N.; Kawasoe, M.; Oka, M. *Koubunshi Kagaku* **1971**, *28*, 610.
(13) Matsumoto, T.; Nakamae, K.; Oka, H.; Kawarai, S. *Sen'i Gakkaishi* **1974**, *30*, 56.
(14) Nishino, T.; Takano, K.; Nakamae, K. *Polymer* **1995**, *36*, 959.
(15) Tashiro, K.; Asanaga, H.; Ishino, R.; Tazaki, R.; Kobayashi, M. *J. Polym. Sci., Part B: Polym. Phys.* **1997**, *35*, 1677.
(16) Moritani, T.; Iwasaki, H. *Macromolecules* **1978**, *11*, 1251.
(17) Akahane, T.; Kazusa, Y.; Nakayasu, H. *Kobunshi Ronbunshu* **1980**, *37*, 383.
(18) Xu, W.; Asai, S.; Sumita, M. *Sen'i Gakkaishi* **1997**, *53*, 174.
(19) Tadokoro, H.; Seki, S.; Nitta, I.; Yamadera, R. *J. Polym. Sci.* **1958**, *28*, 244.
(20) Krimm, S.; Sutherland, G. B. M. *J. Chem. Phys.* **1956**, *25*, 549.
(21) Tashiro, K.; Sasaki, S.; Kobayashi, M. *Macromolecules* **1996**, *29*, 7460.

MA990521A